ELSEVIER

Journal of Structural Geology 27 (2005) 1547–1562

JOURNAL OF STRUCTURAL GEOLOGY

www.elsevier.com/locate/jsg

Relations between surface faulting and granite intrusions in analogue models of strike-slip deformation

Giacomo Corti[a,*], Giovanna Moratti[a], Federico Sani[b]

[a]*CNR—Istituto di Geoscienze e Georisorse, Sezione di Firenze, Consiglio Nazionale delle Ricerche, Via G. La Pira, 4, 50121 Firenze, Italy*
[b]*Dipartimento di Scienze della Terra, Università degli Studi di Firenze, Via G. La Pira, 4, 50121 Firenze, Italy*

Received 27 January 2005; received in revised form 21 April 2005; accepted 9 May 2005
Available online 15 July 2005

Abstract

Analogue models investigating the emplacement of granitic magmas at upper crustal levels during strike-slip deformation are presented in this paper. Variations in parameters such as ratio between horizontal displacement (D_v) and vertical magma upraising (I_v), and the number of feeding points were considered during the experiments. Model results show that a strong interaction between surface faulting and granite intrusions develops during deformation. On one side, magma intrusion influences the sequence of structures development and the final fault pattern. On the other side, magma emplacement is strongly influenced by the syn-intrusion lateral displacement (D_t), which in turn reflects variations in D_v and I_v. For high D_t values (i.e. high displacement velocity or low injection rate), the importance of the horizontal displacement with respect to the vertical magma upraising results in asymmetric and drop-shaped plutons, with a sheared tail elongating in the sense of the strike-slip displacement. In this case, the intrusion long-axis tracks the long-axis of the strain ellipsoid. For low D_t values (i.e. low displacement velocity or high injection rate), the strike-slip displacement is strongly subordinated to the vertical magma upraising and pluton emplacement is controlled by development of tensional shears at the surface. In these conditions, the long-axis of the magmatic bodies lies in the quadrants of compression of the strike-slip deformation and intrusions are apparently dragged in an opposite sense to that imposed by the transcurrent deformation.

Keywords: Granite intrusions; Strike-slip faulting; Pluton shape; Analogue modelling

1. Introduction

Emplacement of granitic bodies along crustal-scale strike-slip faults has been documented in many regions worldwide and major shear zones are considered to represent controlling features in both magma ascent and pluton emplacement processes (e.g. D'Lemos et al., 1992; Hutton and Reavy, 1992; Brown, 1994; Vigneresse, 1995; Román-Berdiel et al., 1997; Rosenberg, 2004 and references therein). Indeed, the final shape of plutons emplaced at rather shallow crustal levels has been suggested to be strongly controlled by deformational features (e.g. Castro, 1987; Hutton, 1988; Pitcher, 1992; Vigneresse, 1995, 1999; Vigneresse and Clemens, 2000). Such a control has been documented in previous experimental models (Román-Berdiel et al., 1997) investigating granite intrusion in a rheologically multilayered upper crust during strike-slip deformation. These models illustrated the importance on intrusion shape of several parameters such as the brittle–ductile layering (e.g. depth and thickness of ductile layers), the position of the feeding pipes, and the volume of injected magma. The experiments showed that the structural pattern has a major influence on the intrusion shape, resulting in typically asymmetric sigmoidal- or lozenge-shaped plutons with a long-axis tracking the local principal stretching direction. Our work aims to implement these previous models by taking into account variations in parameters such as the magma injection rate, the deformation velocity and the total syn-intrusion lateral displacement, which were not considered in the previous works. We focus on the relations between surface faulting and intrusions and investigate in detail how the boundary conditions and the resulting fault pattern influences pluton emplacement.

* Corresponding author. Tel.: +39 055 275 7528; fax: +39 055 290 312.
E-mail address: cortigi@geo.unifi.it (G. Corti).

0191-8141/$ - see front matter © 2005 Elsevier Ltd. All rights reserved.
doi:10.1016/j.jsg.2005.05.011

2. Experimental set-up, materials and scaling

The experiments were performed at the Tectonic Modelling Laboratory of the CNR-IGG settled at the Earth Science Department of Florence University (Italy) and deformed through the use of a pure and simple shear deformation apparatus (Fig. 1). The models with dimensions of 60 cm × 20 cm × 7 cm were built above the basal metal plate of the apparatus. Deformation was obtained through lateral displacement of a 10-cm-wide metal plate creating a velocity discontinuity (VD) in the middle part of the model: with this set-up, half of the model pack was moved horizontally with respect to the other half in order to create a sinistral strike-slip regime of deformation (Fig. 1a and d). Magma intrusion during deformation was allowed by a special injection apparatus consisting of a piston and a magma distribution system made up of pipes and fixed injection points (10 mm in diameter) on the basal metal plate of the deformation apparatus (Fig. 1b–d). The movement of both metal plate and injection piston were driven by electric motors controlled by a control panel. Boundary conditions of the experiments are reported in Table 1. In particular, the horizontal velocity was varied between 0.75 and 10 cm/h, whereas the injection velocity varied from 6 to 80 cm/h; for a constant injected volume, variations in these parameters involved variations in the total amount of syn-intrusion lateral displacement from 0.95 to 15 cm. Experiments with no syn-deformation intrusion were also performed. The volume of analogue magma injected from a single injection point was kept constant (35 cm^3) apart from three models (ME 05, ME 27 and ME 28) characterised by 70 cm^3 of injected volume. The analogue magma was injected through one single point in the central part of model, with the exception of three models (ME 08, ME 09 and ME 11), where the fluid was contemporaneously injected from two or three points aligned parallel to the imposed VD. Similarly to previous experiments on syn-tectonic granite intrusion (e.g. Román-Berdiel et al., 1997, 2000; Benn et al., 1998, 2000), the strike-slip motion was only applied to the models during fluid injection, thus avoiding post-emplacement deformation. This is a reasonable approximation of the natural process, where rather high cooling rates are expected for small magma bodies emplaced at shallow (low-temperature) crustal levels and—once substantially cooled—plutons tend to resist subsequent deformation. This is supported by structural analysis on natural examples showing limited post-intrusive overprint of plutons by subsequent tectonic activity (e.g. Rosenberg, 2004).

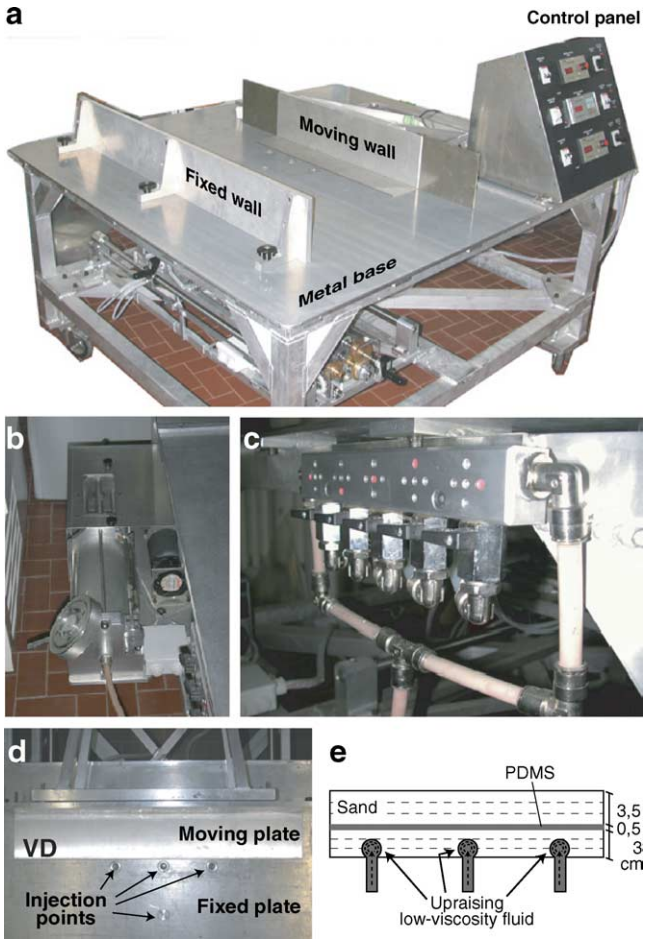

Fig. 1. Details of the experimental set-up. (a) Oblique view of the deformation apparatus; (b) analogue magma injection piston; (c) analogue magma distribution system; (d) top-view showing the injection points, the moving and fixed metal plates and the velocity discontinuity (VD); (e) rheological stratification of models.

2.1. Rheological stratification of the models and analogue materials

Field studies have shown that many granitic plutons emplaced at shallow depths within brittle–ductile rheological systems, such as sedimentary covers containing weak layers (e.g. Román-Berdiel et al., 1997 and references therein). In particular, the emplacement level may be strongly controlled by the presence of soft sedimentary rocks that are able to stop the ascent of granitic magmas allowing them to spread horizontally (Román-Berdiel et al., 1995, 1997). Starting from these observations, the models were intended to simulate intrusion of granitic bodies within a three-layer brittle–ductile system, with a weak ductile horizon embedded within two brittle layers (Fig. 1e). To this purpose, the brittle behaviour was reproduced in the experiments by using dry Qz-sand, characterised by grain size <250 μm, angle of internal friction of $\sim 39°$, cohesion of ~ 65 Pa and density of ~ 1550 kg m^{-3}. In order to better visualise and analyse in detail the internal brittle deformation, different layers of coloured sand were introduced as horizontal markers within the sand-pack. The weak ductile layer was simulated by using polydimethylsiloxane (PDMS), a transparent silicone with density of 965 kg m^{-3} and Newtonian behaviour at strain rates $<3\times10^{-3}$ s^{-1} (Weijermars, 1986). In the current experiments, estimates of

Table 1
Parameters of model deformation

Model	Displacement velocity, D_v (cm/h)	Injection velocity, I_v (cm/h)	D_v/I_v	Number of intrusion	Injected volume (cm^3)	Exp. duration (min)	Total displacement, D_t (cm)
No intrusion							
ME 10	5	–	–	–	–	90	7.5
ME 12	10	–	–	–	–	90	15
Constant injection velocity, variable displacement velocity							
ME 15	0.75	30	0.02	1	35	90	1.15
ME 13	1	30	0.03	1	35	90	1.5
ME 13bis	1	30	0.03	1	35	90	1.5
ME 14	1.5	30	0.05	1	35	90	2.25
ME 16	2	30	0.07	1	35	90	3
ME 07	2.5	30	0.08	1	35	90	3.75
ME 25	3.6	30	0.12	1	35	90	5.5
ME 06	5	30	0.17	1	35	90	7.5
ME 18	7.5	30	0.25	1	35	90	11.25
ME 04	10	30	0.33	1	35	90	15
Constant displacement velocity, variable injection velocity							
ME 19	2	6	0.33	1	35	420	14
ME 24	2	8	0.25	1	35	335	11
ME 20	2	12	0.17	1	35	230	7.9
ME 26	2	17	0.12	1	35	160	5.4
ME 21	2	25	0.08	1	35	110	3.7
ME 23	2	40	0.05	1	35	68	2.3
ME 22	2	60	0.03	1	35	45	1.5
ME 17	2	80	0.02	1	35	35	1.2
Multiple injection points							
ME 11	2.5	30	0.08	3	105 (35×3)	90	3.75
ME 08	5	30	0.17	3	105 (35×3)	90	7.5
ME 09	5	30	0.17	2	70 (35×2)	90	7.5
Increased injected volume							
ME 27	2	60	0.03	1	70	90	3
ME 28	5	60	0.08	1	70	90	7.5
ME 05	5	30	0.17	1	70	180	15

Dimensions of the PDMS layer: length 45 cm, width 20 cm; height 0.5 cm. Sand thickness: (below PDMS) 3 cm; (above PDMS) 3.5 cm. Total model thickness: 7 cm.

the strain rates (based on the displacement velocity and the width of the ductile shear zone) yield maximum values of $\sim 8\times10^{-4}\ s^{-1}$, supporting that rheology of the PDMS did not significantly depart from the Newtonian behaviour within the shear zone. A viscosity of $\sim 3\times10^{4}$ Pa s was measured with a coni-cylindrical viscometer at room temperature of $\sim 22\,^{\circ}$ C. This weak layer was embedded in the sand-pack 3 cm above the injection point and the basal metal plate of the deformation apparatus. The intrusions were modelled with a mixture of silicone (Mastic Silicone Rebodissant 29, produced by CRC, France) and oleic acid (4:1% in weight) resulting in a low-viscosity Newtonian fluid with viscosity of $\sim 7\times10^{2}$ Pa s and density of $\sim 1060\ kg\ m^{-3}$.

2.2. Scaling

The experiments were scaled taking into considerations the conditions of geometrical, dynamical, kinematical and rheological similarity outlined by Hubbert (1937), Ramberg (1981) and Weijermars and Schmeling (1986). In particular, the models were built with a length scaling ratio of 10^{-5}, such that 1 cm in the experiments corresponds to 1 km in nature (Table 2). Considering this geometrical scaling ratio and the reduction factors of density ($\rho^* = \rho_{mod}/\rho_{nat} \sim 0.4$) and gravity ($g^* = g_{mod}/g_{nat} = 1$), the corresponding model to nature ratio of stresses was of the order of 4×10^{-6}.

We adopted a time ratio of $\sim 1.5\times10^{-9}$ (1 h in the models represents $\sim$80,000 yr in nature); this implies a scaling factor of the linear injection velocity of $\sim 6.6\times10^{3}$, such that injection of 30 cm/h scales to $\sim$40 cm/yr in nature (Table 2; see also Román-Berdiel et al., 1997). The use of linear injection rates of this order of magnitude allows us to obtain magma driving pressures comparable with those inferred for natural conditions (Román-Berdiel et al., 1995, 1997). The scaling ratio of viscosity is $\sim 6\times10^{-15}$, resulting in a scaled viscosity of $\sim 5\times10^{18}$ Pa s for the weak ductile layer, and $\sim 10^{17}$ Pa s for the granitic magma. Thus, the silicone–oleic acid mixture was only able to simulate a high viscosity crystal-rich magma (e.g. Román-Berdiel et al., 1997; Benn et al., 1998, 2000); however, this mixture was still suitable to model a significant strength

Table 2
Scaled parameters of model deformation

Model	Scaled displacement velocity, D_v (cm/yr)	Scaled injection velocity, I_v (cm/yr)[a]	D_v/I_v	Injected volume (km^3)	Duration (yr)	Scaled total displacement, D_t (km)
No intrusion						
ME 10	6.6	–	–	–	1.1×10^5	7.5
ME 12	13.3	–	–	–	1.1×10^5	15
Constant injection velocity, variable displacement velocity						
ME 15	1.0	39.9	0.02	35	1.1×10^5	1.15
ME 13	1.3	39.9	0.03	35	1.1×10^5	1.5
ME 14	2.0	39.9	0.05	35	1.1×10^5	2.25
ME 16	2.7	39.9	0.07	35	1.1×10^5	3
ME 07	3.3	39.9	0.08	35	1.1×10^5	3.75
ME 25	4.8	39.9	0.12	35	1.1×10^5	5.5
ME 06	6.6	39.9	0.17	35	1.1×10^5	7.5
ME 18	10.0	39.9	0.25	35	1.1×10^5	11.25
ME 04	13.3	39.9	0.33	35	1.1×10^5	15
Constant displacement velocity, variable injection velocity						
ME 19	2.7	8.0	0.33	35	5.3×10^5	14
ME 24	2.7	10.6	0.25	35	4.2×10^5	11
ME 20	2.7	16.0	0.17	35	2.9×10^5	7.9
ME 26	2.7	22.6	0.12	35	2.0×10^5	5.4
ME 21	2.7	33.2	0.08	35	1.4×10^5	3.7
ME 23	2.7	53.2	0.05	35	8.6×10^4	2.3
ME 22	2.7	79.8	0.03	35	5.7×10^4	1.5
ME 17	2.7	106.4	0.02	35	4.4×10^4	1.2
Multiple injection points						
ME 11	3.3	39.9	0.08	105 (35×3)	1.1×10^5	3.75
ME 08	6.6	39.9	0.17	105 (35×3)	1.1×10^5	7.5
ME 09	6.6	39.9	0.17	70 (35×2)	1.1×10^5	7.5
Increased injected volume						
ME 27	2.7	79.8	0.03	70	1.1×10^5	3
ME 28	6.6	79.8	0.08	70	1.1×10^5	7.5
ME 05	6.6	39.9	0.17	70	2.3×10^5	15

[a] For a scaled diameter of the feeding pipe of 1 km.

contrast between the low viscosity melt fraction and the host rocks (Cruden et al., 1995). Indeed, as noted by Román-Berdiel et al. (1997), for slow displacement velocities the silicone–oleic acid mixture offers a negligible resistance and scaling for viscosity is not critical.

3. Experimental results: surface fault pattern

3.1. Evolution of deformation—no analogue magma injection

The evolution of deformation in models with no fluid injection is illustrated by the analysis of model ME 10, characterised by a displacement velocity of 5 cm/h. This model showed a typical sequence of structure development, as observed in the classical strike-slip physical experiments (e.g. Tchalenko, 1970; Naylor et al., 1986). In particular, lateral displacements up to 2.5 cm were accommodated by development of Riedel (R) shears trending at ~15° to the basal VD (Fig. 2a). Increasing deformation was taken up by development of faults subparallel to the velocity discontinuity (Y shears), which started forming after 2.5 cm of horizontal displacement (Fig. 2a). These Y shears grew laterally accommodating an increasing part of the horizontal deformation. Together with later P shears (forming at ~15° to the basal VD, but with an opposite trend with respect to the R shears), the low-angle faults connected and subsequently overprinted the Riedel shears, which progressively became inactive. As in previous models (e.g. Naylor et al., 1986), the final deformation pattern was characterised by a major throughgoing deformed zone with anastomosing faults defining shear lenses (Fig. 2a; horizontal displacement: 7.5 cm).

The pattern of doming in the ductile layer (Fig. 2a, bottom panel) displays the development of oblique folds—trending 10–20° clockwise with respect to the direction of displacement—with a left-stepping en-échelon arrangement in a narrow zone of intensive deformation. These folds were superimposed on axial undulations, characterised by a right-stepping en-échelon arrangement with the main axis oriented about 10° counterclockwise relative to the displacement direction. Similar features of ductile deformation were previously observed in analogue experiments by Dauteuil and Mart (1998).

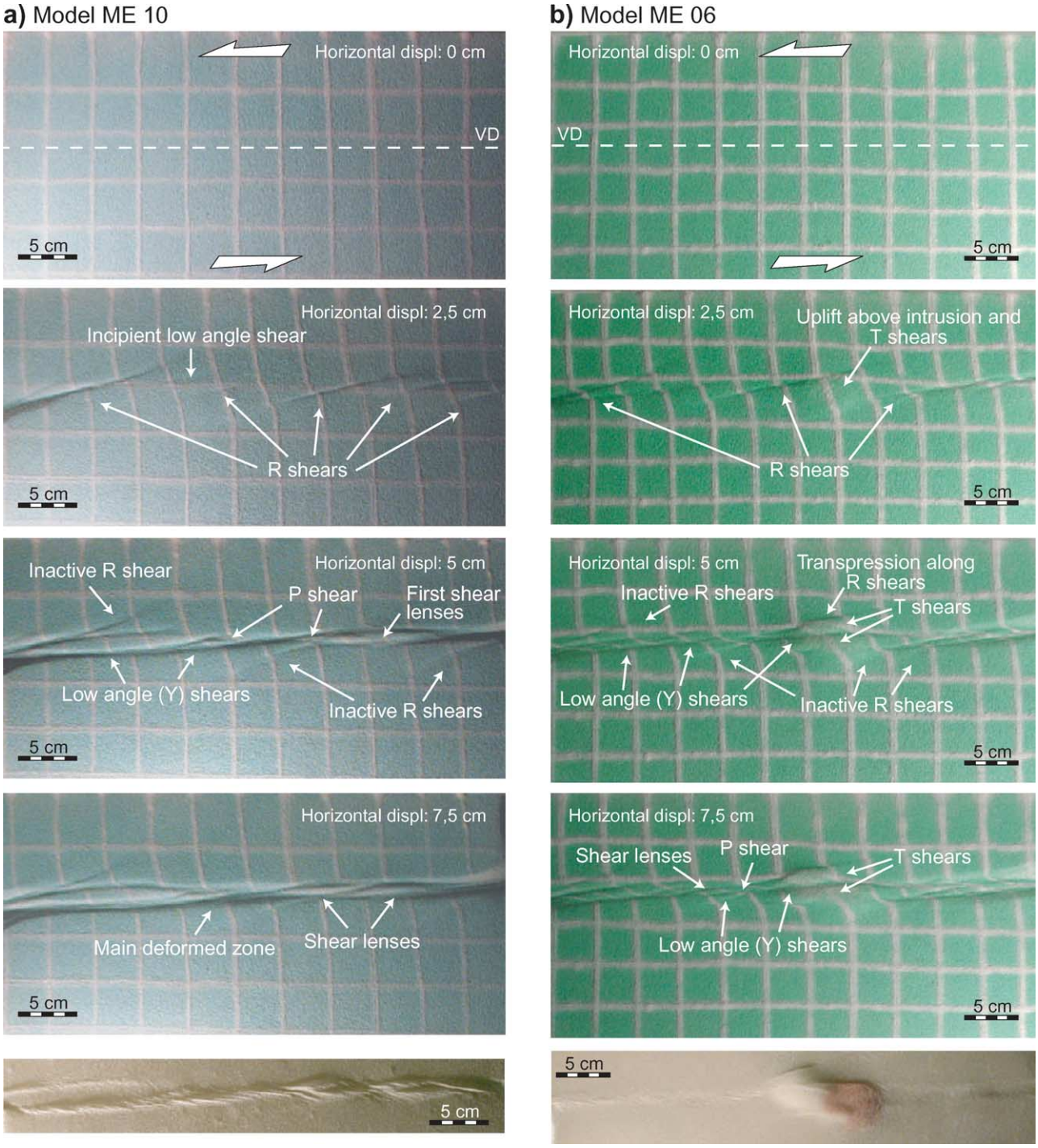

Fig. 2. Evolution of the surface fault pattern in models ME 06 (displacement velocity: 5 cm/h; velocity of injection: 30 cm/h) and ME 10 (displacement velocity: 5 cm/h; no injection). For both models, the lower panels show the final top-view photo of the ductile PDMS layer once the cover sand has been removed.

3.2. Evolution of deformation—analogue magma injection

The evolution of deformation in models with analogue magma injection is illustrated by the analysis of model ME 06, characterised by displacement velocity of 5 cm/h and injection of 30 cm/h. In this model, the initial stages of deformation were still characterised by development of R shears trending at ~15° to the basal VD (Fig. 2b). In this case, however, the syn-deformation magma intrusion resulted in the uplift of the model surface in a narrow area above the fluid injection point. This uplift, in turn, determined the development of normal faults and transpressive kinematics along the terminations of some Riedel structures (Fig. 2b). Notably, intrusion determined a

widening of the deformed zone in correspondence to the analogue magma injection point. Further deformation led to the linking of early R shears to form low angle Y faults and finally to the development of a low-angle main deformed zone with P shears and shear lenses (Fig. 2b; horizontal displacement: 7.5 cm), as observed in the previous model ME 10.

In the case of syn-deformation intrusion, ductile deformation was still accommodated by development of arrays of en-échelon minor folds; in this case, however, maximum folding of the ductile layer occurred above the intrusion area and the development of axial undulations was strongly reduced (Fig. 2b, bottom panel).

3.3. Influence of the ratio between displacement velocity and injection velocity on the surface fault pattern

Model results suggest that the surface fault pattern during intrusion was strongly influenced by the ratio between displacement and injection velocity (D_v/I_v), as illustrated by comparison of models ME 09 and ME 11 characterised by constant injection velocity (30 cm/h), but different horizontal displacement velocity (5 and 2.5 cm/h, respectively; Fig. 3). Particularly, in the case of low displacement velocity–injection velocity ratio (model ME 11, $D_v/I_v = 0.08$), deformation was initially taken up by normal faults with no development of R shears. This resulted from the dominance of intrusion-induced uplift over lateral displacement. Increasing the displacement velocity (model ME 09, $D_v/I_v = 0.17$) resulted in early development of R shears with subordinated normal faults, as a consequence of decreasing the importance of intrusion-induced uplift with respect to strike-slip deformation. This initial difference in deformation was maintained at the end of lateral displacement: normal faults were indeed well developed and rotated during deformation in model ME 11, where they accommodated $\sim$1.5 cm of horizontal extension, with maximum vertical throw on single structures of $\sim$5 mm; extensional structures only accommodated a minor part of displacement ($<$0.5 cm) in model ME 09 (Fig. 3).

The influence of the D_v/I_v ratio on the development of normal faults vs. R shears is additionally illustrated in the graph of Fig. 4. In this graph, the percentage of deformation accommodated by normal faults or R shears for a fixed lateral displacement of 1 cm is plotted against the horizontal velocity in models characterised by a constant

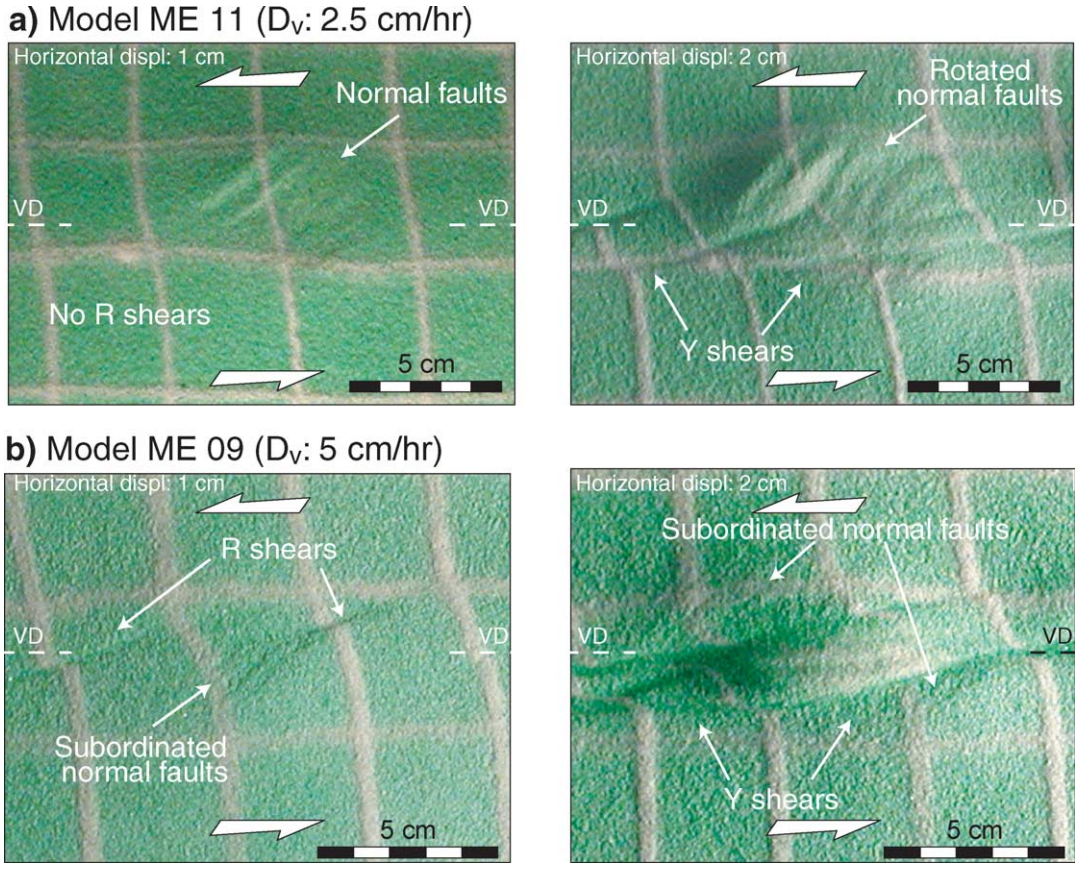

Fig. 3. Influence of the ratio between displacement velocity and injection velocity on the surface fault pattern, illustrated by comparison of top-view photos of models ME 09 and ME 11 characterised by constant injection velocity (30 cm/h), but different horizontal displacement velocity (5 and 2.5 cm/h, respectively). For both models, left and right panels correspond to horizontal displacement of 1 and 2 cm, respectively. See text for details.

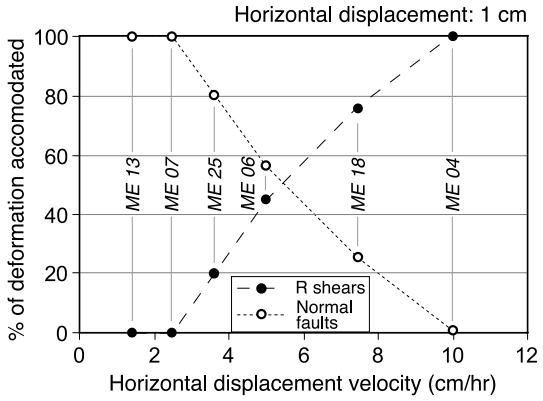

Fig. 4. Percentage of displacement (measured in the horizontal plane) accommodated by normal faults and R shears plotted vs. horizontal displacement velocity for a fixed lateral displacement of 1 cm. Note that with increasing displacement velocity, the strike-slip deformation accommodated by R shears increases. For horizontal displacement velocities $\leq$2.5 cm/h, deformation is entirely accommodated by normal faults; for horizontal displacement velocities $\geq$10 cm/h, deformation is entirely accommodated by R shears.

injection velocity. The graph clearly shows that for low displacement velocities (up to $\sim$3 cm/h), normal faults accommodate the whole strike-slip deformation. Increasing the lateral velocity, the amount of deformation taken up by R shears linearly increases and finally (for displacement velocities of $\sim$10 cm/h) these structures entirely accommodate the transcurrent motion (Fig. 4).

3.4. Influence of multiple intrusions on surface fault pattern

Comparison of models characterised by a single injection point and models with two or three feeding pipes is illustrated in Fig. 5. Analysis of the evolution of structures and the final surface pattern suggests that syn-deformation multiple intrusions resulted in a more complex structural pattern with respect to models with no or only one analogue magma intrusion.

Indeed, the strike-slip motion was accommodated by an increasing number of faults (characterised by a mean—tip to tip—length decrease) increasing the number of intrusions. Increase in the fault number was related to the strong strain localisation in correspondence to the magmatic bodies and resulted on one side from the increase in the number of normal faults above intrusions and on the other side from an increase in the segmentation of the major faults (which is more pronounced for low values of lateral displacement). As observed in Section 3.2, syn-deformation intrusion determined a widening of the main deformed zone above the analogue magma injection point; this effect was more marked in models characterised by two or three feeding pipes, leading to a general increase in the area of the model surface affected by the strike-slip deformation (Fig. 5b and c).

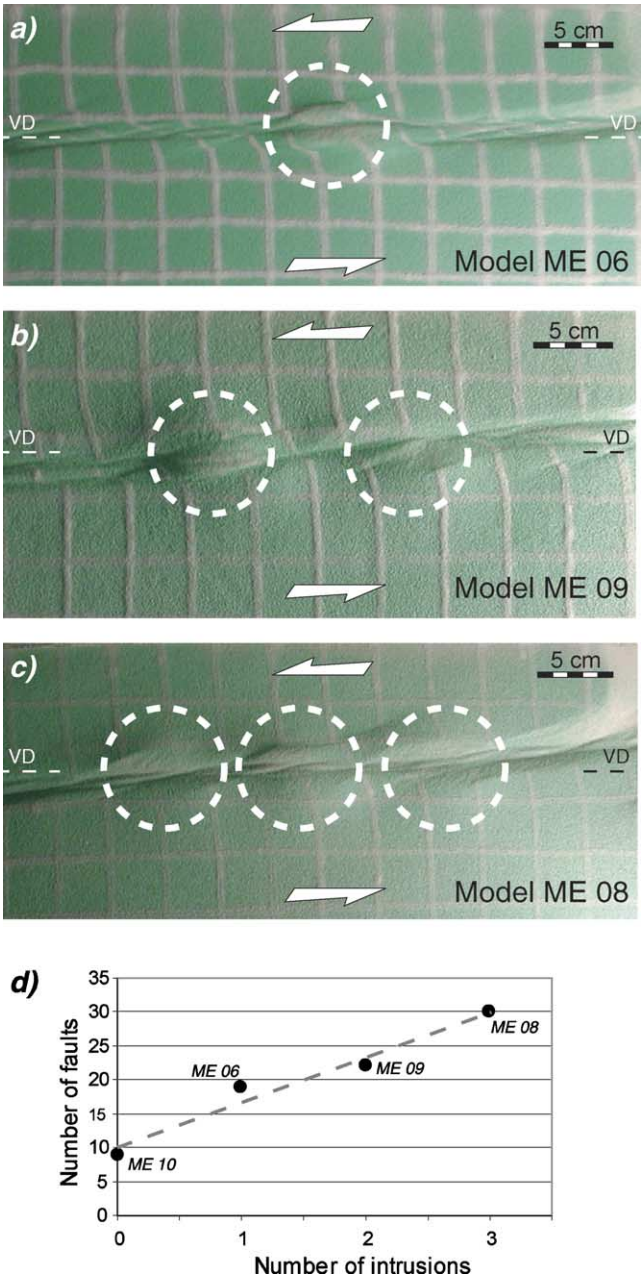

Fig. 5. Influence of multiple intrusions on the surface fault pattern. (a)–(c) Top-view photos of models ME 06, 08 and 09 (horizontal displacement is 3 cm); dotted circles indicate the regions above the injection points subjected to intrusion-related surface uplift. (d) Plot of number of faults vs. number of intrusions for the different models.

4. Experimental results: intrusion shape

Influence of strike-slip deformation on pluton shape was analysed in the current experiments by varying the horizontal displacement velocity (D_v), the magma injection rate (I_v) and the volume of injected material. In particular, nine experiments were conducted with different D_v (from 0.75 to 10 cm/h), keeping a constant injection rate of 30 cm/h; conversely, in eight experiments we varied I_v (from 6 to 80 cm/h), with constant displacement rate of

2 cm/h (Table 1). Since in both experimental series the volume of injected material was kept constant, variation in D_v and I_v involved variations in the total amount of syn-intrusion lateral displacement (D_t). Finally, three models were performed with an increased volume of injected magma (70 cm^3 instead of 35 cm^3) in order to test the influence—for similar D_v/I_v ratios—of the total displacement D_t on the final shape of intrusions.

In the different experiments, intrusion occurred in correspondence of the main shear zone; space for the upraising magma was mainly created by pushing aside the weak layer and lifting of the overburden (Fig. 6a), as evidenced by uplift of the model surface above the injection point (see Figs. 2, 3 and 5). The final shape of intrusions was strongly influenced by deformation, with development of asymmetric, drop-shaped or elongated plutons (Fig. 6b), whose geometrical characteristics were controlled by boundary conditions (see Sections 4.1–4.3). The magma analogue intruded the PMDS layer, although major accumulation occurred below the ductile layer (Fig. 6a and b). Only in the case of model ME 05, characterised by large injected volume (70 cm^3) and large lateral displacement (15 cm), has the magma analogue pierced the ductile layer and reached the model surface (Fig. 6c). In this case, the shape of the magma body was strongly influenced by faults, being the intrusion boundaries of the intrusion sub-parallel to P and R shears observed on the model surface (Fig. 6c; e.g. Román-Berdiel et al., 1997).

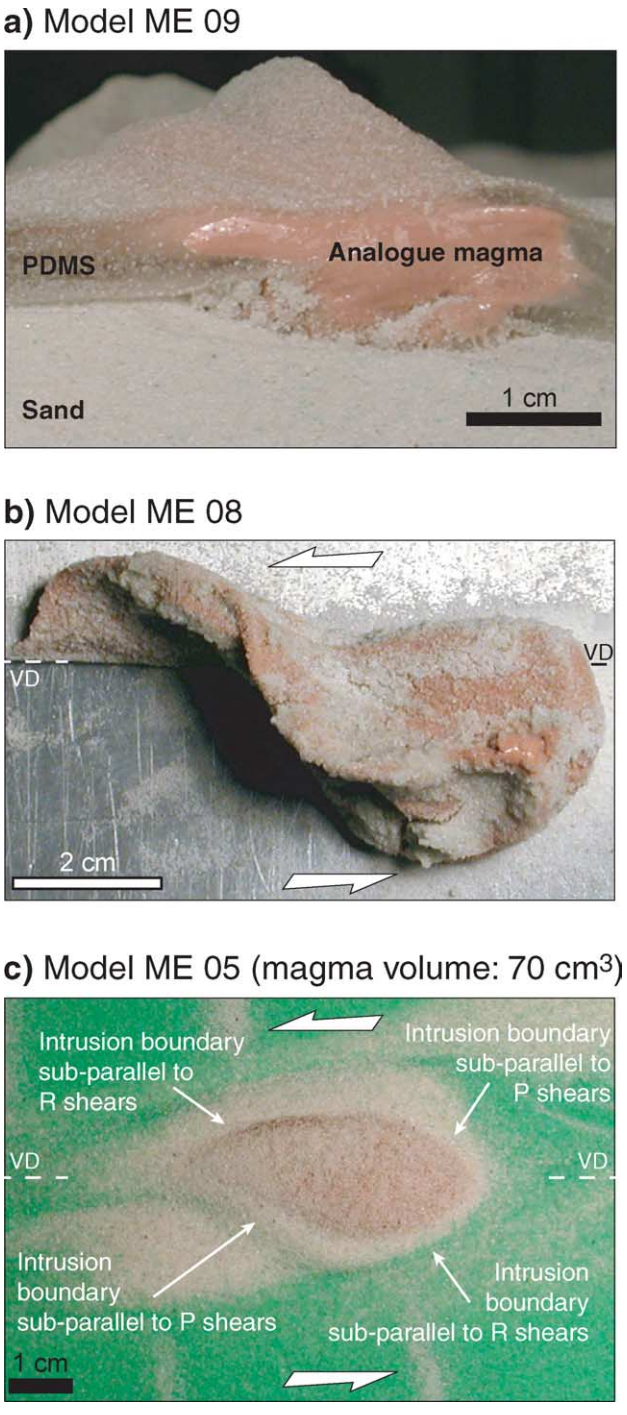

Fig. 6. Characteristics of analogue magma intrusions. (a) Model cross-section showing the analogue magma intruding the PMDS layer (model ME 09); (b) top-view photo of an asymmetric, drop-shaped intrusion (model ME 08); (c) top-view photo of model ME 05 showing emplacement at surface of the analogue magma in the case of large injected volume (70 cm^3 instead of 35 cm^3).

4.1. Constant injection velocity, variable displacement velocity

The shape of intrusions in relation to the different boundary conditions of deformation is analysed by describing some principal geometrical features such as the (length/width) aspect ratio and the trend of the pluton main axis, as schematically illustrated in Fig. 7. As stated in Section 3, syn-deformation intrusions were influenced by the deformational parameters (Figs. 8–10).

In the case of constant injection velocity ($I_v = 30$ cm/h), intrusions were controlled by the different deformation velocity (D_v), in turn controlling the total syn-intrusion displacement (D_t; Fig. 8a). For $D_v > \sim 1$ cm/h and $D_t >$ 2 cm, intrusions were characterised by a final shape defining an asymmetric drop, with the main body located beside the main shear zone and a sheared tail trailing behind the

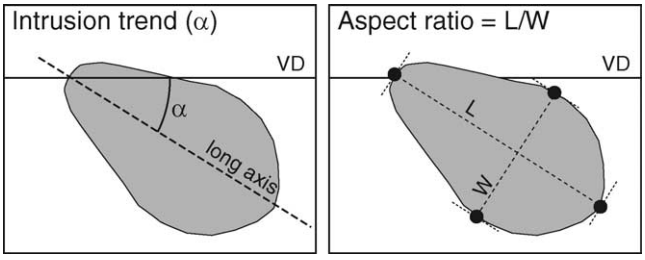

Fig. 7. Geometrical parameters of intrusions analysed in this work. The intrusion trend is defined by the angle α, representing the angle (measured clockwise) that the intrusion long-axis forms with the direction of the velocity discontinuity, VD. The aspect ratio is calculated as the ratio between length (L) and width (W) of intrusions.

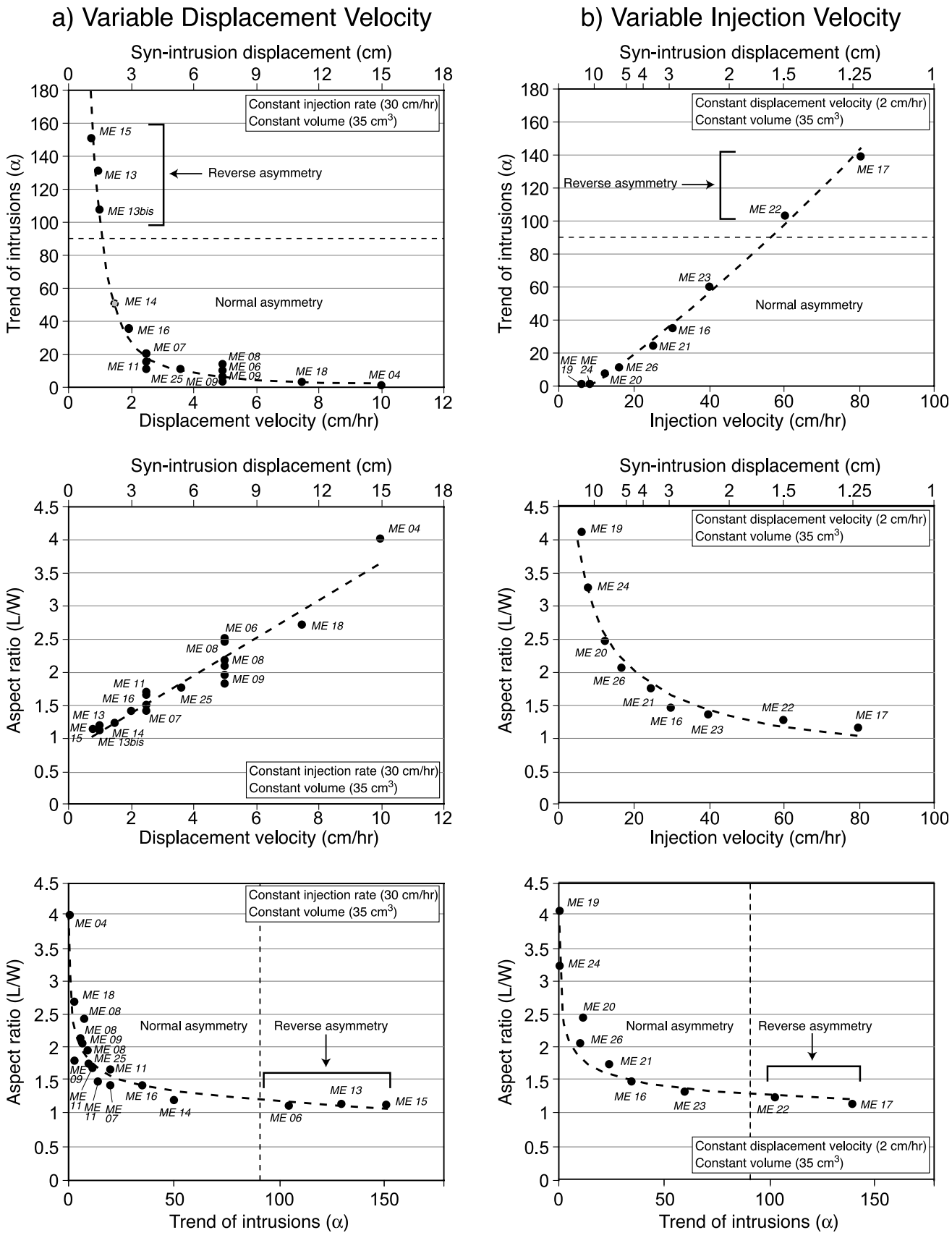

Fig. 8. Graphs of the experimental results for models with (a) constant injection rate and variable displacement velocity and (b) constant displacement velocity and variable injection rate. See text for details.

intrusion, well developed for $D_t > 3$ cm (Fig. 9a–c). The intrusion tail was localised above the VD, within the shear zone, and constituted a narrow analogue magma body, with vertical dimensions similar to the wider parts of the intrusions (Fig. 9a and b). Increasing the deformation velocity, the length of the tail increased (Fig. 9a–c); consequently, a similar increase was observed in the relative volume of the tail with respect to the main intrusion body, from ~15% for low D_v and D_t (e.g. model ME 11; $D_v = 2.5$ cm; $D_t = 3.75$ cm) to ~50% for high D_v and D_t (e.g. model ME 04; $D_v = 10$ cm; $D_t = 15$ cm). The asymmetric pluton shape resulted in a high aspect ratio and the main axis of intrusions forming an angle $\alpha < 90°$ with the VD. This indicates that plutons tended to parallelise the VD, being dragged according to the strike-slip displacement (e.g. models ME 04, 08, 11; Fig. 9a–c); we refer to this situation as 'normal asymmetry' of the intrusion main axis with respect to the basal VD.

Decreasing the deformation velocity and the total displacement, the angle α increased, whereas the aspect ratio of intrusions displayed a constant decrease (Fig. 8a). For $D_v \leq 1$ cm/h and $D_t < 2$ cm, the orientation of the pluton main axis with respect to the VD was characterised by an angle $\alpha > 90°$ (Figs. 8a and 9d). In this case, the intrusion main axis was apparently dragged in a direction opposite to that imposed by the strike-slip deformation (e.g. model ME 13; Fig. 9d), a situation that we term 'reverse asymmetry'.

Plot of intrusion trend vs. aspect ratio shows that intrusions with normal asymmetry were characterised by higher elongation (and aspect ratio) with respect to plutons with reverse asymmetry. Indeed, in the normal asymmetry field ($\alpha < 90°$) the aspect ratio normally varied between ~1.5 and ~4; conversely, in the reverse asymmetry field ($\alpha > 90°$) the aspect ratio was normally ~1.1–1.3.

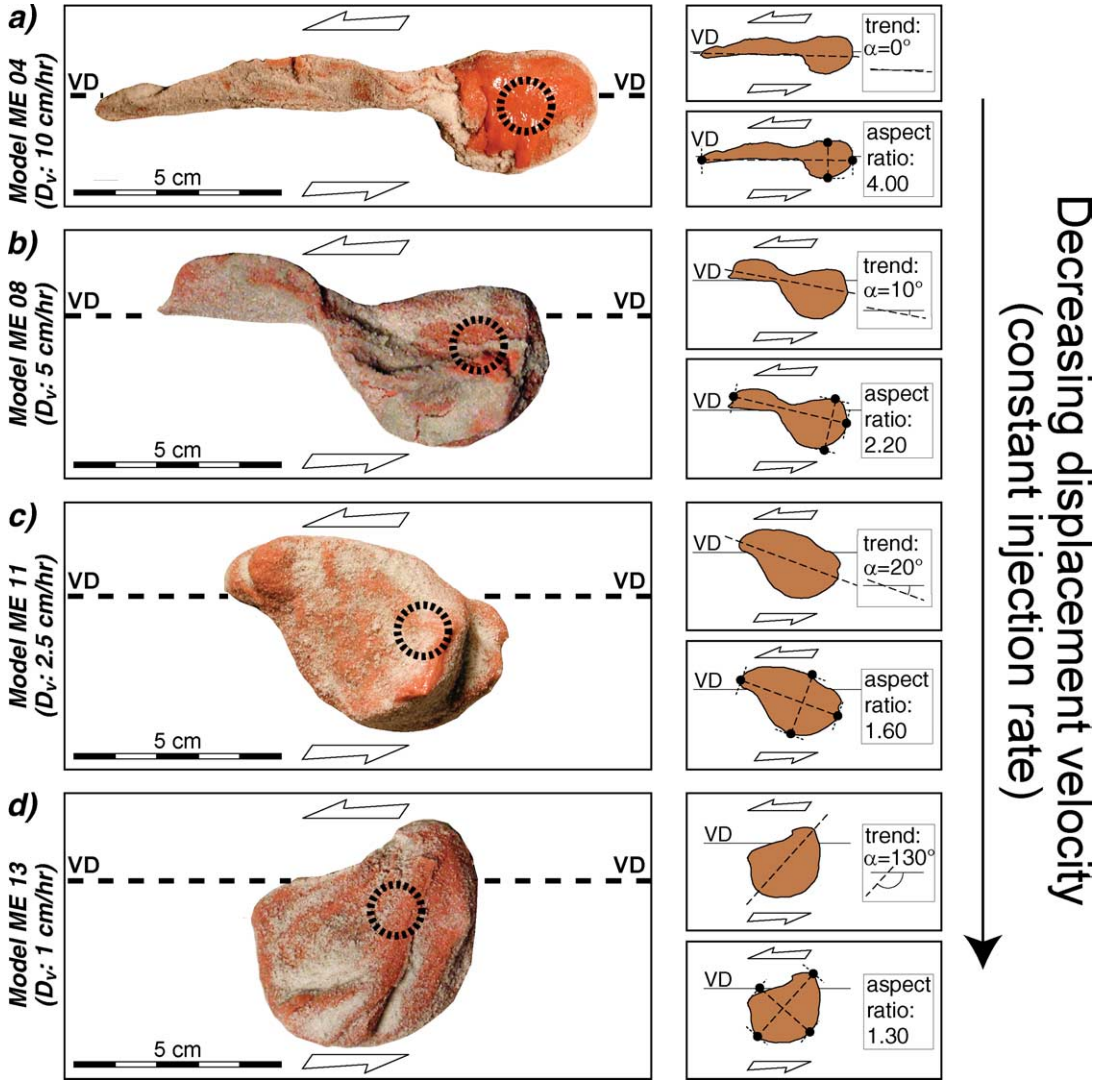

Fig. 9. Variable shape of intrusions in relation to different displacement velocities (for a constant injection rate). Dotted circles indicate the position of the magma injection point of the apparatus. See text for details.

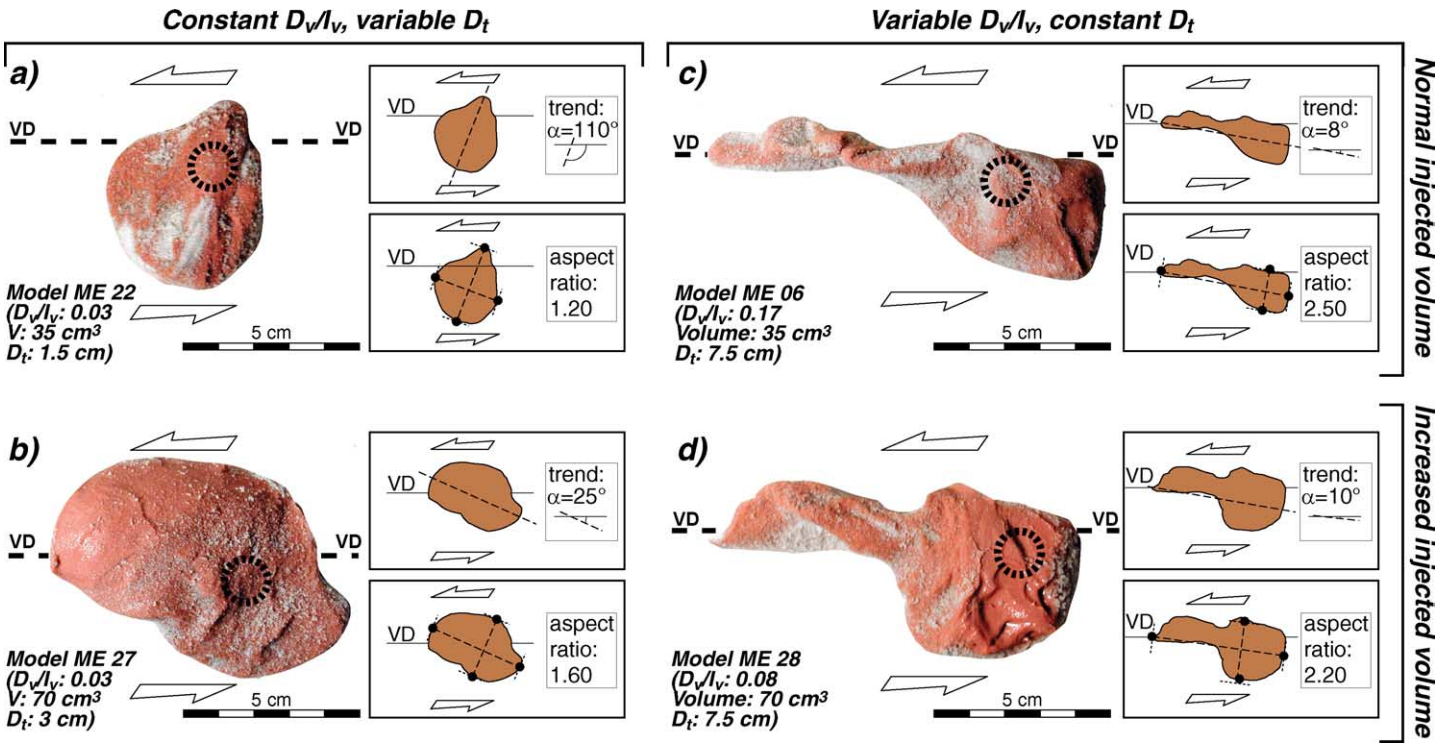

Fig. 10. Comparison of experiments performed with normal (35 cm^3) and increased (70 cm^3) injected volume of analogue magma. (a) and (b) Models with similar D_v/I_v ratios (=0.03), but different syn-intrusion displacement (D_t) resulting from the different magma volume. (c) and (d) Models with similar D_t (=7.5 cm), but different D_v/I_v ratios. See text for details.

4.2. Constant displacement velocity, variable injection velocity

Fig. 8b portrays the results of experiments conducted with constant displacement velocity ($D_v = 2$ cm/h) and variable injection velocity, I_v.

In this case, low injection velocities (I_v between 6 and 40 cm/h) and high lateral displacement (D_t between 2 and 10 cm) resulted in normal asymmetry of intrusions, with constant increase of the angle α with increasing I_v. For $I_v > 60$ cm/h ($D_t > 2$ cm), a reverse asymmetry was observed, with angles $\alpha > 90°$. The intrusion aspect ratio decreased, increasing the injection velocity I_v; similarly to what has been described in the previous section, intrusions with normal asymmetry were characterised by higher aspect ratio (~1.3–4) with respect to plutons with reverse asymmetry (~1.1–1.2).

4.3. Increased injected volume and the influence of syn-intrusion lateral displacement

The above results suggest that the competition between the horizontal displacement and vertical magma injection controls the final magma emplacement process; in particular, the syn-intrusion lateral displacement D_t has a major influence on the shape of intrusions. This influence was tested by performing experiments with increased injected volume, which allowed us to compare results of models characterised by similar D_v/I_v ratios, but different D_t resulting from the different volumes of injected material (Fig. 10a and b; Table 1). This comparison showed that—for similar D_v/I_v ratios—intrusion resulted in reverse asymmetry for $D_t < 2$ cm (e.g. model ME 22, $D_v/I_v = 0.03$, volume = 35 cm^3, D_t = 1.5 cm; Fig. 10a) and normal asymmetry for $D_t > 2$ cm (e.g. model ME 27, $D_v/I_v = 0.03$, volume = 70 cm^3, D_t = 3 cm; Fig. 10b). Overall, influence of the syn-intrusion lateral displacement on the shape of intrusions is displayed in the graphs of Fig. 11a and b, where the intrusion trend and the aspect ratio are plotted against D_t. The graphs show a general increase in the angle α decreasing D_t (i.e. decreasing the importance of lateral displacement with respect to magma injection; Fig. 11a). Intrusions with normal asymmetry are observed for $D_t >$ 2 cm, whereas the field of reverse asymmetry is restricted to $D_t < 2$ cm (Fig. 11a). Similarly, increasing the D_t leads to a regular increase in the aspect ratio (Fig. 11b); intrusions with normal asymmetry are characterised by higher aspect ratio with respect to those characterised by reverse asymmetry. Notably, for similar syn-intrusion displacement an increase in the injected volume (and a decrease in the D_v/I_v ratio) led to an increase in the angle α and a decrease in the aspect ratio (Fig. 10c and d). Fig. 11c summarises the above results by showing conditions that are expected to lead to normal or reverse asymmetry in a graph of D_t vs. injection duration, reported for both experimental and scaled natural conditions. The two fields of intrusions shape are separated by a transition line corresponding to $D_t \sim 2$ cm and ~2 km for experiments and nature, respectively.

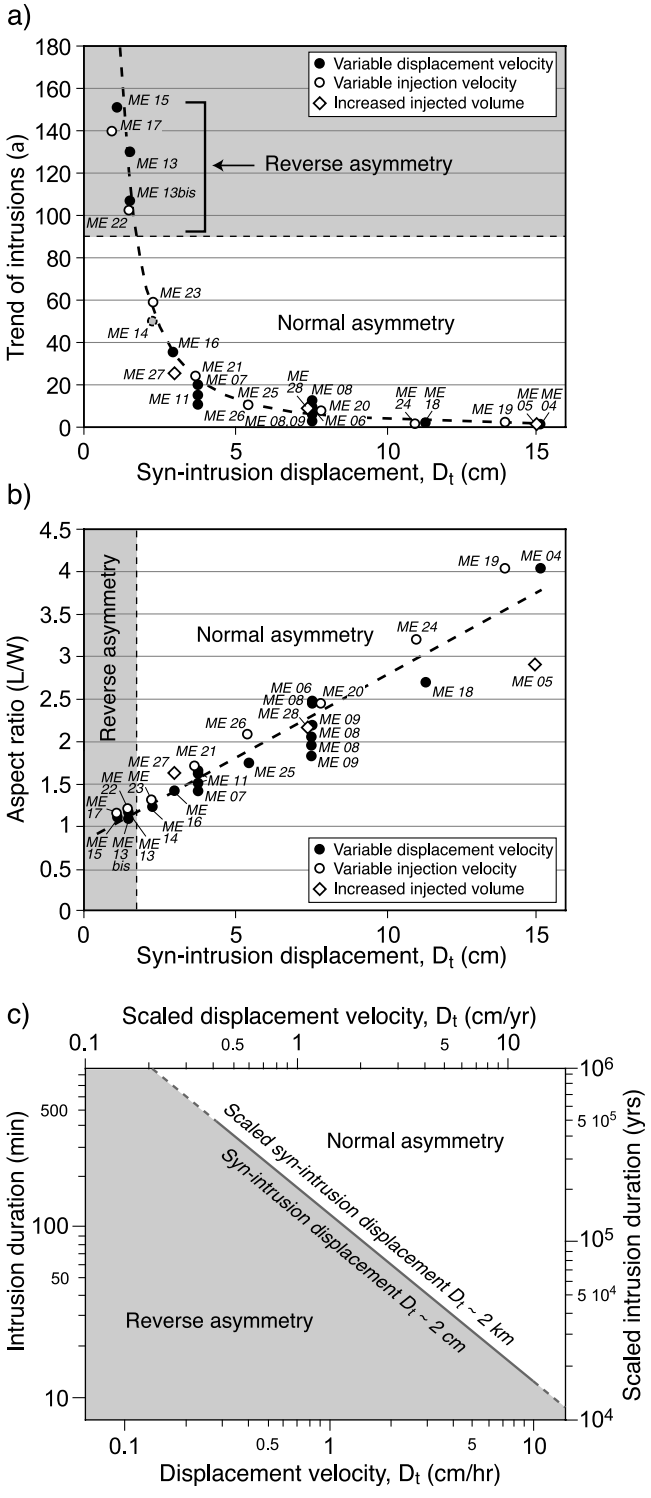

Fig. 11. (a) and (b) Experimental results expressed in terms of variable syn-intrusion displacement D_t. (c) Fields of normal and reverse asymmetry of intrusions in a graph of D_t vs. injection duration, reported for both experimental and scaled natural conditions. See text for details.

5. Discussion and comparison with natural examples

The current laboratory experiments provide support that strong interactions between surface faulting and granite intrusions in the upper crust may develop during strike-slip deformation. On one side, intrusions affect the structures development and modify surface fault pattern; on the other side, boundary conditions of deformation and the resulting structural patterns have a strong control on pluton emplacement.

5.1. Relations between surface faulting and granite intrusions

With no magma involved in the process, the strike-slip deformation generates a sequence of deformation from early development of R shears that progressively link to form a throughgoing main deformed zone composed of low angle (Y) shears and P shears, as typically observed in previous models (e.g. Naylor et al., 1986). Folding of the ductile layer accommodates deformation in the overlying brittle layer (Dauteuil and Mart, 1998). Syn-deformation intrusion modifies the sequence of structures development by inducing uplift above the injection point accommodated by formation of normal faults and reduced slip along R shears. Development of normal faults is favoured by a decrease in displacement velocity with respect to injection rate, resulting in a dominance of intrusion-induced uplift over lateral displacement. In these conditions, the ductile layer is mainly folded above the upraising magma. Notably, introducing multiple injection points in the system results in a more complex structural pattern, with a greater number of (shorter) faults forming in response to a strong strain localisation in correspondence of the magmatic bodies.

5.2. Influence of deformation on pluton emplacement

Intrusion of the analogue magma occurred in correspondence of the main shear zone, with space created by lateral displacement of the weak layer and lifting of the overburden causing marked surface uplift, analogously to that observed in previous models (Román-Berdiel et al., 1995, 1997; Benn et al., 1998, 2000). Similar processes have been inferred to contribute to create space for incoming magmas in nature (e.g. Petford et al., 2000). Model results provide support that magma emplacement is strongly influenced by boundary conditions of deformation, with the final intrusion shape being controlled by the syn-intrusion lateral displacements, in turn reflecting the competition between the horizontal displacement and the vertical magma upraising. In particular, for $D_t > \sim 2$ cm (i.e. high displacement velocity or low injection rate; Fig. 11c), intrusions are commonly asymmetric and drop-shaped, with a sheared tail elongating in the sense of the strike-slip displacement (normal asymmetry). In these conditions, the intrusion tail is localised above the VD, within the shear zone, and constitutes a subvertical analogue magma body; conversely, the main body is located beside the main shear zone and is more tabular and gently dipping than the tail. The asymmetric shape results from a horizontal displacement important with respect to the vertical magma upraising with the emplacement being controlled by the strong shear strain gradient at the vicinity of the main fault zone (e.g. Román-Berdiel et al., 1997). In this case, the main axis of the intrusion lies in the extensional quadrants of the strike-slip deformation (Fig. 12a), with the long-axis of intrusion parallelising the VD, increasing the shear strain, as observed in previous modelling (Román-Berdiel et al., 1997). Notably, the asymmetric pluton shape resembles the geometry of winged porphyroclasts obtained in simple-shear deformation experiments (e.g. Hanmer and Passchier, 1991).

For $D_t < \sim 2$ cm (i.e. low displacement velocity or high injection rate; Fig. 11c), the horizontal displacement is strongly subordinated to the vertical magma upraising: as a consequence, plutons do not elongate according to the strike-slip motion; rather, they are apparently dragged in a direction opposite to that imposed by the strike-slip deformation (reverse asymmetry). In this case, the intrusions parallel the trend of normal faults, testifying the control exerted by these structures on the final emplacement which occur in the low lithostatic stress areas of the experimental system (e.g. Benn et al., 2000); the long-axis of the magmatic bodies lies in the quadrants of compression of the strike-slip deformation (Fig. 12b). Notably, these findings extend the results of Román-Berdiel et al. (1997), which only observed and described intrusion shapes in the normal asymmetry field, with the experiments restricted to large syn-intrusion displacements ($D_t > 9.6$ cm). Differently from the current models, in their experiments the long-axis of intrusions always tracked the long-axis of the bulk strain ellipsoid.

5.3. Implications for the process of syn-tectonic granite emplacement in nature

Although the models were characterised by some intrinsic limitations mainly related to the impossibility of correctly reproducing thermal and rheological conditions (e.g. thermal weakening of the country rocks; magma rheological properties, involving changes in rheology and strength during cooling and crystallisation; Román-Berdiel et al., 1997; Corti et al., 2003), the experimental findings may have important relevance for the natural process of granite intrusions during transcurrent faulting. In particular, normal and reverse asymmetry are to be expected where high and low syn-intrusion lateral displacements characterise the emplacement in strike-slip zones (Fig. 11c). The first case may be characteristic of plutons accumulating in small increments over large time spans (e.g. Glazner et al., 2004): in this case, rates of granite construction may approach those of tectonic processes; given the large duration of

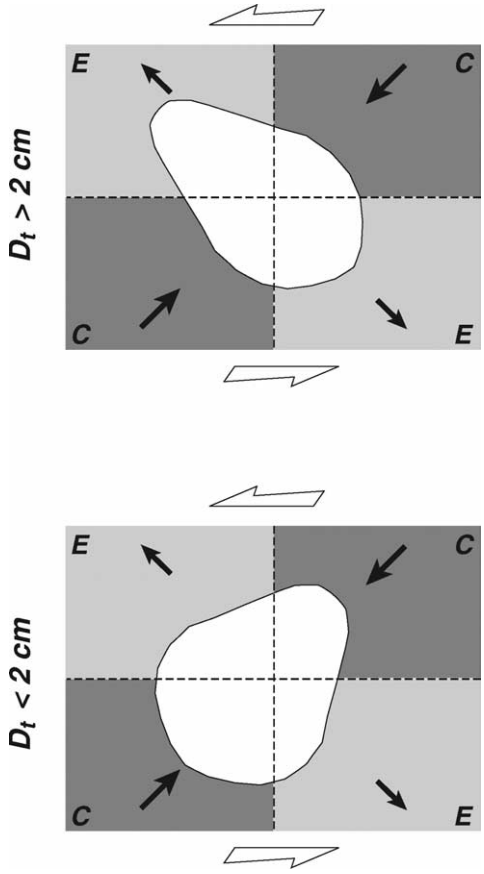

Fig. 12. Elongation of intrusions in the compressional (*C*) or extensional (*E*) quadrants of the strike-slip deformation.

intrusion, large displacements along major faults may effectively control the final pluton shape with the development of sheared tails tracing the strike-slip deformation and high aspect ratios. Conversely, reverse asymmetry may characterise plutons with a geologically rapid (or very rapid) emplacement (e.g. Petford et al., 2000): in these conditions, rates of granite accumulation may be several orders of magnitude higher than those of tectonic processes; the strike-slip offset on faults is insufficient to control intrusion shape, resulting in a long-axis orientation opposite to the transcurrent displacement and low aspect ratios. From the above observations, it results that the asymmetry and elongation of syn-tectonic plutons are not always diagnostic of the shear-sense along strike-slip faults, being the intrusion shape highly sensitive to the boundary conditions of deformation. In addition, the spatial relationships between emplacement-related structures and the intrusion vary according to the level of exposure (Benn et al., 2000); for instance, the tensional faults controlling the emplacement of reverse asymmetry plutons are expected not to be preserved if erosion acted enough to expose granites at surface. These processes may alter the statistical associations between faults and plutons (e.g. Paterson and Schmidt, 1999), as a close spatial relationship between strike-slip-related structures and syn-tectonic intrusions might not be evident. This obviously further complicates the interpretation of emplacement processes based on geological and/or geophysical data (e.g. Benn et al., 2000).

Classical examples of highly asymmetric, drop-shaped intrusions include the syn-tectonic granites of the South Armorican Shear Zone, which have been compared with analogue modelling results by Román-Berdiel et al. (1997). As noted by these authors, these plutons result from strong shearing along the main fault zone, with the development of a sheared tail that elongates according to the shear-sense. Thus, in these conditions, the magma injection rate is subordinated to the strike-slip displacement resulting in a normal asymmetry ($\alpha < 90°$) and high intrusion aspect ratios ($L/W > 2$; Fig. 13a). Similarly, intrusions with normal asymmetry characterise the Tertiary syn-tectonic magmatism developed along the Periadriatic Fault System (PFS) in the Alps (Rosenberg, 2004, and references therein). There, strong control on magma ascent and emplacement exerted by major shear zones resulted in highly asymmetric and elongated intrusions. As in the current models, the final

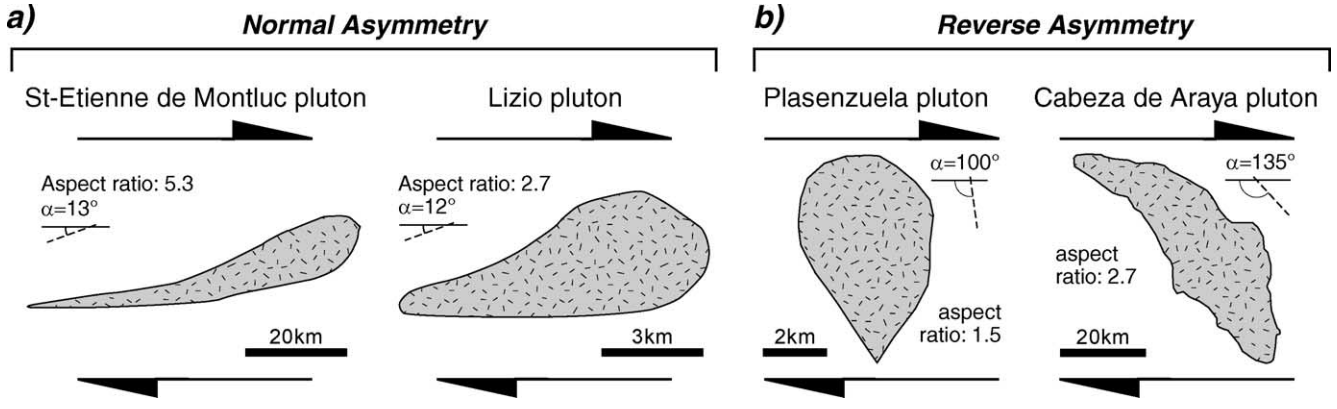

Fig. 13. Shape of plutons in natural examples. (a) Normal asymmetry associated with high aspect ratios in the syn-tectonic granites of the South Armorican Shear Zone (after Román-Berdiel et al., 1997); (b) reverse asymmetry with low aspect ratios in the plutons of the Central Extremadura batholith (after Fernández and Castro, 1999). Note that the aspect ratio of the Cabeza de Araya intrusion ($L/W \approx 2.7$) possibly results from coalescence of different magmatic pulse during pluton emplacement (e.g. Vigneresse and Bouchez, 1997; Fernández and Castro, 1999).

emplacement of these magmatic bodies occurred by extrusion from the PFS into the adjacent country rocks, with the intrusion level controlled by major rheological contacts (Rosenberg, 2004). Similarly to experimental results, intrusions are characterised by high aspect ratio (up to 1000) and a sheared tail (made up of steep to subvertical sheets) within the main shear zone; in contrast, the main plutons outcrop beside the PFS and are characterised by gently dipping contacts with the country rocks (Rosenberg, 2004).

Natural examples of reverse asymmetry may include the syn-tectonic plutons of the Central Extremadura batholith in the Iberian Massif (Fernández and Castro, 1999; Fig. 13b). In this batholith, intrusion of magmatic bodies results from very high feeding rates and filling times on the order of 10^2 yr; in these conditions (lateral displacement subordinated to magma injection), the pluton geometry is not directly controlled by shearing along the strike-slip fault and strong control by tensional fractures is observed (e.g. Fernández and Castro, 1999; Fig. 13b). As in the analogue experiments, intrusions are characterised by an angle $\alpha > 90°$ and low aspect ratios; thus, the pluton shape does not trace the shear-sense of the transcurrent fault zone and a reverse asymmetry occurs (Fig. 13b).

6. Conclusions

Laboratory analogue models were used to investigate the process of granite intrusions at upper crustal levels during strike-slip faulting. The influence of some boundary conditions such as the ratio between displacement velocity and injection rate and the number of feeding points were investigated in the experimental series. Model results suggest that a strong interaction between surface faulting and granite intrusion in the upper crust may develop. In particular, the main conclusions supported by the current experimental work are:

(1) syn-deformation intrusions modify the sequence of structures development and the final surface fault pattern;
(2) multiple magma injection points result in a more complex structural pattern, with strain localisation in correspondence of the magmatic bodies;
(3) consistently with previous models (e.g. Román-Berdiel et al., 1997), intrusion of the analogue magma occurs within the main shear zone, with space created by lateral displacement of the weak layer and lifting of the overburden;
(4) the shape of the magmatic body was controlled by the syn-intrusion lateral displacement (D_t), reflecting variations in the displacement velocity (D_v) and the magma injection rate (I_v). High D_t values (i.e. high horizontal displacement velocity or low vertical magma upraising) result in asymmetric, drop-shaped plutons, with a sheared tail elongating in the sense of the strike-slip displacement (normal asymmetry). In this case, the intrusion long-axis tracks the long-axis of the strain ellipsoid. For low D_t values (i.e. low displacement velocity or high magma injection rate), pluton emplacement is controlled by development of tensional faults at surface. In these conditions, the long-axis of the magmatic bodies lies in the quadrants of compression of the strike-slip deformation and intrusions are apparently dragged in a direction opposite to that imposed by the transcurrent deformation giving rise to a reverse asymmetry of the pluton shape.

Acknowledgements

We thank the journal reviewers K. Benn and T. Román-Berdiel for the detailed, constructive comments that helped to improve the manuscript. F. Mazzarini and G. Musumeci are warmly thanked for the comments and the stimulating discussions. Research funded by CNR-IGG and University of Florence funds.

References

Benn, K., Odonne, F., de Saint-Blanquat, M., 1998. Pluton emplacement during transpression in brittle crust: new views from analog experiments. Geology 26, 1079–1082.

Benn, K., Odonne, F., Lee, S.K.Y., Darcovich, K., 2000. Analogue models of pluton emplacement during transpression in brittle and ductile crust. Transactions of the Royal Society of Edinburgh: Earth Sciences (Hutton IV special issue) 91, 111–121.

Brown, M., 1994. The generation, segregation, ascent and emplacement of granite magma. Earth-Science Reviews 36, 83–130.

Castro, A., 1987. On granitoid emplacement and related structures. A review. Geologische Rundschau 76, 101–124.

Corti, G., Bonini, M., Conticelli, S., Innocenti, F., Manetti, P., Sokoutis, D., 2003. Analogue modelling of continental extension: a review focused on the relations between the patterns of deformation and the presence of magma. Earth-Science Reviews 63, 169–247.

Cruden, A.R., Koyi, H., Schmeling, H., 1995. Diapiric basal entrainment of mafic into felsic magma. Earth Planetary Science Letters 131, 321–340.

Dauteuil, O., Mart, Y., 1998. Analogue modelling of faulting pattern, ductile deformation, and vertical motion in strike-slip fault zones. Tectonics 17, 303–310.

D'Lemos, R.S., Brown, M., Strachan, R.A., 1992. Granite magma generation, ascent and emplacement within a transpressional orogen. Journal of the Geological Society of London 149, 487–496.

Fernández, C., Castro, A., 1999. Pluton accommodation at high strain rates in the upper continental crust. The example of the Central Extremadura batholith, Spain. Journal of Structural Geology 21, 1143–1149.

Glazner, A.F., Bartley, J.M., Coleman, D.S., Gray, W., Taylor, R.Z., 2004. Are plutons assembled over millions of years by amalgamation from small magma chambers? GSA Today, 14 (doi: 10.1130/1052-5173(2004)014<0004:APAOMO>2.0.CO;2).

Hanmer, S., Passchier, C., 1991. Shear-sense indicators: a review. Geological Survey of Canada. Paper 90-17.

Hubbert, M.K., 1937. Theory of scaled models as applied to the study of geological structures. Geological Society of America Bulletin 48, 1459–1520.

Hutton, D.H.W., 1988. Granite emplacement mechanisms and tectonic controls: inferences from deformation studies. Transactions of the Royal Society of Edinburgh: Earth Sciences 79, 245–255.

Hutton, D.H.W., Reavy, R.S., 1992. Strike-slip tectonics and granite petrogenesis. Tectonics 11, 960–967.

Naylor, M.A., Mandl, G., Sijpesteijn, C.H.K., 1986. Fault geometries in basement-induced wrench faulting under different initial stress states. Journal of Structural Geology 7, 737–752.

Paterson, S.R., Schmidt, K.L., 1999. Is there a close relationship between faults and plutons? Journal of Structural Geology 21, 1131–1142.

Petford, N., Cruden, A.R., McCaffrey, K.J.W., Vigneresse, J.-L., 2000. Granite magma formation, transport and emplacement in the Earth's crust. Nature 408, 669–673.

Pitcher, W.S., 1992. The Nature and Origin of Granite. Blackie Academy Press, London.

Ramberg, H., 1981. Gravity, Deformation and the Earth's Crust, 2nd ed. Academic Press, London.

Román-Berdiel, T., Gapais, D., Brun, J.-P., 1995. Analogue models of laccolith formation. Journal of Structural Geology 17, 1337–1346.

Román-Berdiel, T., Gapais, D., Brun, J.-P., 1997. Granite intrusion along strike-slip zones in experiment and nature. American Journal of Science 297, 651–678.

Román-Berdiel, T., Aranguren, A., Cuevas, J., Tubía, J.M., Gapais, D., Brun, J.P., 2000. Experiments on granite intrusions in transtension. In: Vigneresse, J.L., Mart, Y., Vendeville, B. (Eds.), Salt, Shale and Igneous Diapirs in and Around Europe Special Publications, vol. 174. Geological Society, London, pp. 21–42.

Rosenberg, C.L., 2004. Shear zones and magma ascent: a model based on a review of the Tertiary magmatism in the Alps. Tectonics 23, TC2003. doi:10.1029/2003TC001526.

Tchalenko, J.S., 1970. Similarities between shear zones of different magnitudes. Geological Society of America Bulletin 81, 1625–1640.

Vigneresse, J.L., 1995. Control of granite emplacement by regional deformation. Tectonophysics 249, 173–186.

Vigneresse, J.L., 1999. Should felsic magmas be considered as tectonic objects, just like faults or folds? Journal of Structural Geology 21, 1125–1130.

Vigneresse, J.L., Bouchez, J.L., 1997. Successive granitic magma batches during pluton emplacement: the case of Cabeza de Araya (Spain). Journal of Petrology 38, 1767–1776.

Vigneresse, J.L., Clemens, J.D., 2000. Granitic magma ascent and emplacement: neither diapirism nor neutral buoyancy. In: Vigneresse, J.L., Mart, Y., Vendeville, B. (Eds.), Salt, Shale and Igneous Diapirs in and Around Europe Special Publications, vol. 174. Geological Society, London, pp. 1–19.

Weijermars, R., 1986. Flow behaviour and physical chemistry of bouncing putties and related polymers in view of tectonic laboratory applications. Tectonophysics 124, 325–358.

Weijermars, R., Schmeling, H., 1986. Scaling of Newtonian and non-Newtonian fluid dynamics without inertia for quantitative modelling of rock flow due to gravity (including the concept of rheological similarity). Physics of the Earth and Planetary Interiors 43, 316–330.